Geol. Mag. **155** (*1*), *2018, pp. 109–118.* © *Cambridge University Press 2016*
doi:10.1017/S0016756816000972

Chromite chemistry as an indicator of petrogenesis and tectonic setting of the Ranomena ultramafic complex in north-eastern Madagascar

C. ISHWAR-KUMAR*, V.J. RAJESH†, B.F. WINDLEY‡, T. RAZAKAMANANA§, T. ITAYA¶, E.V.S.S.K. BABU|| & K. SAJEEV*#

*Centre for Earth Sciences, Indian Institute of Science, Bangalore 560012, India
†Department of Earth and Space Sciences, Indian Institute of Space Science and Technology, Thiruvananthapuram 695547, India
‡Department of Geology, The University of Leicester, Leicester LE1 7RH, UK
§Département de Sciences Naturelles, Université de Toliara, BP.185, Toliara 601, Madagascar
¶Japan Geochronology Network (NPO), 2–5 Nakahima, Naka Ward, Okayama 703–8252, Japan
||CSIR - National Geophysical Research Institute, Hyderabad 500007, India

(*Received* 6 March 2016; *accepted* 20 September 2016; *first published online* 28 November 2016)

Abstract – The Ranomena ultramafic complex in NE Madagascar consists of layered gabbro, harzburgite, orthopyroxenite, clinopyroxenite, garnet websterite and chromitite-layered peridotite. This study of the Ranomena chromite chemistry aims to better understand the petrogenesis and palaeotectonic environment of the complex. The chromite from the Ranomena chromitite is unzoned/weakly zoned and has a Cr# (Cr/(Cr + Al)) of 0.59–0.69, a Mg# (Mg/(Fe + Mg)) of 0.37–0.44, and low Al_2O_3 (15–23 wt %) suggesting derivation from a supra-subduction zone arc setting. Calculation of parental melt composition suggests that the parental magma composition of the Ranomena chromitite was similar to that of a primitive tholeiitic basalt formed at a high degree of mantle melting, suggesting the parental melt composition was equivalent to that of an island-arc tholeiite (IAT). The parental magma of the Ranomena chromite had a FeO/MgO ratio of 0.9 to 1.8, suggesting arc derivation. The parental magma was Al- and Fe-rich, similar to a tholeiitic basaltic magma. The composition of orthopyroxene from the chromitite indicates a crystallization temperature range of 1250–1300 °C at 1.0 GPa. The chemistry of the chromite in the Ranomena chromitite further suggests that the complex formed in a supra-subduction zone arc tectonic setting.

Keywords: Chromite, chromitite, Ranomena ultramafic complex, Betsimisaraka suture, NE Madagascar.

1. Introduction

Chromite (chromian spinel, Cr-spinel) commonly occurs as an accessory phase in mafic-ultramafic rocks and as the major mineral in chromitite (e.g. Irvine, 1965; Arai, 1992, 1994; Rollinson, Appel & Frie, 2002). Chromite is one of the earliest minerals to crystallize from a mafic-ultramafic magma and a sensitive indicator of primary magma/melt compositions; it has therefore been widely used to understand the petrogenesis of its host rocks (Irvine, 1965; Cameron, 1975; Roeder, Campbell & Jamieson, 1979; Arai, 1994; Barnes & Hill, 1995; Rollinson, 1995, 2008; Barnes, 2000; Mukherjee *et al.* 2010; Arai *et al.* 2011; González-Jiménez *et al.* 2014*a*,*b*, 2015; Zhou *et al.* 2014; Ishwar-Kumar *et al.* 2016*a*). Interpretation of chromite chemistry becomes difficult if it has undergone alteration (Evans & Frost, 1975; Eales, Wilson & Reynolds, 1988; Burkhard, 1993) or post-crystallization re-equilibration (Hamlyn & Keays, 1979; Scowen, Roeder & Heltz, 1991). Metamorphosed chromite is generally richer in iron than its unmetamorphosed equivalent because of Mg–Fe exchange with silicates (Barnes, 2000). The degree of mantle melting, magma composition, crystallization sequence and pressure–temperature conditions can vary significantly among different geotectonic regimes, leading to distinctive variations in the composition of chromite (Ahmed *et al.* 2005; Karipi *et al.* 2007; Aswad, Aziz & Koyi, 2011). The chemistry of chromite is therefore a diagnostic indicator of different tectonic settings (Irvine, 1967; Arai, 1980, 1994; Barnes & Roeder, 2001; Arai *et al.* 2011; Dharma Rao *et al.* 2013).

The Precambrian basement of Madagascar (Besairie, 1967) is made up of several Mesoarchaean–Neoproterozoic crustal blocks separated by shear/suture zones. The Betsimisaraka suture zone in NE Madagascar separates the Neoarchean Antananarivo block in the west from the Mesoarchean Antongil-Masora blocks in the east (Collins *et al.* 2003; Kröner *et al.* 2000; Collins & Windley, 2002; Raharimahefa & Kusky, 2009). The Betsimisaraka suture zone consists predominantly of paragneisses

#Author for correspondence: sajeev@ceas.iisc.ernet.in

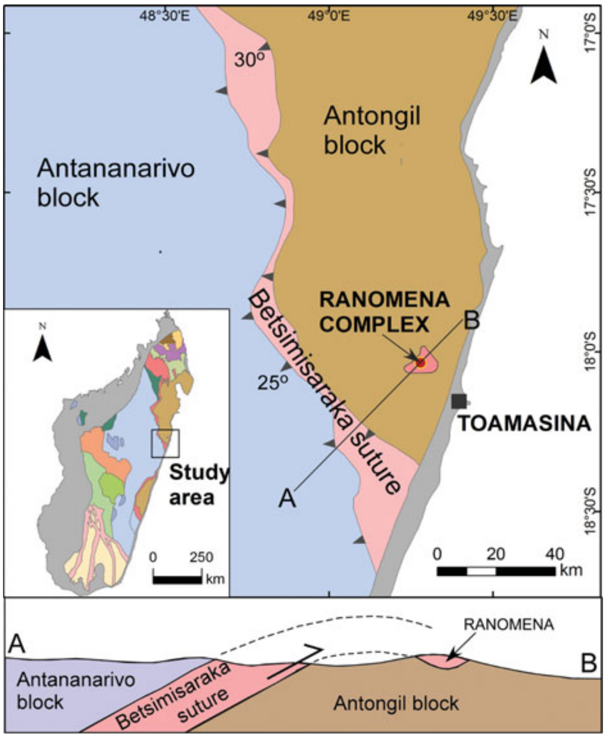

Figure 1. (Colour online) Geological map of the Ranomena complex and surrounding region, showing part of the west-dipping Betsimisaraka suture, the Antananarivo block and the Antongil block in NE Madagascar. The Ranomena complex (modified after Collins and Windley, 2002; Bauer & Key, 2005; Raharimahefa & Kusky, 2009) is situated in a slice of the Betsimisaraka suture that has been thrust eastwards over the Antongil block. A schematic geological cross-section along the AB line is given below the map.

and mica-schists that dip shallowly to the west. In recent studies, the existence and exact position, shape and age of the Betsimisaraka suture has become controversial (Tucker *et al.* 1999, 2011, 2014; Key *et al.* 2011; Ishwar-Kumar *et al.* 2013, 2015,2016*b*; Rekha *et al.* 2013; Rekha, Bhattacharya & Prabhakar, 2014; Ratheesh-Kumar *et al.* 2015). The Ranomena complex consists of layered gabbro, harzburgite, orthopyroxenite, clinopyroxenite, garnet websterite and chromitite-layered harzburgite (Hottin, 1969; Bauer & Key, 2005; Grieco, Merlini & Cazzaniga, 2012; Grieco *et al.* 2014). The chromite in the chromitite may potentially reveal valuable information about its petrogenesis and tectonic setting. In this study, we present chromite chemical data from the Ranomena chromitite to constrain its petrogenesis, parental magma composition and crystallization temperature in order to better understand its tectonic setting.

2. Geological background

The Ranomena ultramafic complex (hereafter Ranomena complex) is located *c.* 25 km NW (17° 45′ S; 48° 06′ E) of Toamasina (Tamatave) town in northeastern Madagascar (Fig. 1) (Kröner *et al.* 2000; Collins & Windley, 2002). It is a *c.* 700 m long, 300 m wide lens that consists of harzburgite, orthopyroxenite, clinopyroxenite, chromitite-layered harzburgite and two pyroxene-hornblende gabbro (Hottin, 1969), the chromitites occurring between alternating layers of harzburgite and pyroxenite (Grieco, Merlini & Cazzaniga, 2012; Grieco *et al.* 2014). The Ranomena complex occurs in garnet-sillimanite paragneiss, amphibolite and *c.* 3100 Ma migmatitic gneiss (Bauer & Key, 2005). The Betsimisaraka belt, which consists largely of high-strain paragneisses that contain emerald mineralization, graphite-rich schists and several major lenses of garnet-bearing mafic-ultramafic rocks (Hottin, 1969; Besairie, 1970), is widely regarded as a west-dipping suture zone between the Antongil and Masora blocks to the east and the Antananarivo block to the west (Kröner *et al.* 2000; Collins & Windley, 2002; Collins *et al.* 2003; Raharimahefa & Kusky, 2009). Tucker *et al.* (2011) suggested an alternative model, according to which the zone was occupied by a sedimentary basin (the Manampotsy Group) that was deposited during the period 840–760 Ma and was inter-thrust with the margins of the Antananarivo and Antongil–Masora blocks during 560–520 Ma. According to these authors there was an ocean on the site of the Manampotsy basin, which was destroyed during Neoarchean time.

The Betsimisaraka suture contains several relict mafic-ultramafic complexes (Hottin, 1969). From a study of platinum-group minerals (PGM), Grieco, Merlini & Cazzaniga (2012) and Grieco *et al.* (2014) interpreted the Ranomena complex as a continental layered/stratiform intrusion. The Antananarivo block to the west of the suture mainly consists of Neoarchean (*c.* 2500 Ma) granulite to amphibolite facies orthogneisses intruded by arc-generated 820–740 Ma aged granitic rocks and gabbros (Kröner *et al.* 1999, 2000; Tucker *et al.* 1999, 2011, 2014). On the eastern side of the suture is a remnant, thin quartzite-dominated shelf that has been imbricated with gneisses from the under-thrusted Archean Antongil craton (Windley *et al.* 1994; Collins & Windley, 2002; Schofield *et al.* 2010). Figure 1 shows that the Ranomena complex is situated in a small slice of gneisses that has been thrust eastwards from the west-dipping Betsimisaraka suture over the Antongil block.

3. Petrography and mineral chemistry

3.a. Petrographic and textural characteristics

The Ranomena chromitite mainly consists of *c.* 85 vol. % chromite, *c.* 10 vol. % olivine and *c.* 5 vol. % orthopyroxene (Fig. 2a–c). Chromite grains are mostly euhedral; grain size varies over the range 0.01–0.1 mm and is characterized by a cumulate texture. Anhedral olivine and orthopyroxene are main inter-cumulus minerals.

3.b. Mineral compositions

The constituent minerals of the Ranomena chromitite were analysed with a Cameca SX-100 electron-probe micro-analyser at the Geological Survey of

https://doi.org/10.1017/S0016756816000972 Published online by Cambridge University Press

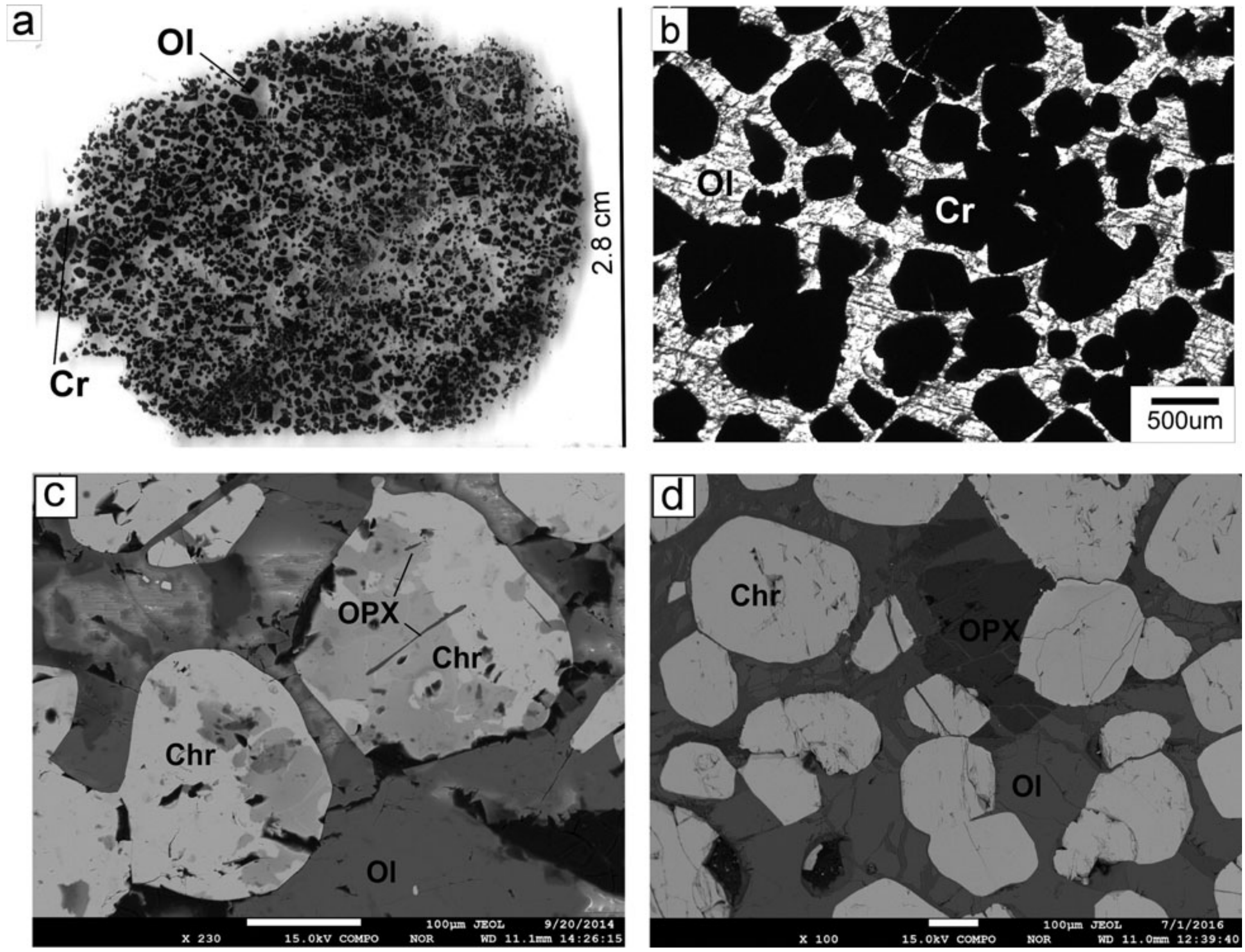

Figure 2. Thin section micrographs. (a) Chromitite from the Ranomena complex, showing the massive texture of a chromitite layer. (b) Chromitite sample from the Ranomena complex, plane polarized light. (c) Backscattered electron image of chromite grains showing the mineral inclusions and textures of chromitite. (d) Backscattered electron image of chromitite showing chromite, olivine and orthopyroxene grains. Cr – chromite; Ol – olivine; OPX – orthopyroxene.

India, Bangalore, India, a JEOL JX8900 electron probe micro-analyser in the Okayama University of Science, Okayama, Japan (Tsujimori *et al.* 1998), and a Cameca SX-100 electron probe micro-analyser at the National Geophysical Research Institute, Hyderabad, India. The inclusions in chromite were studied with a JEOL JXA 8300 at the Advanced Facility for Microscopy and Microanalysis, Indian Institute of Science, Bangalore, India. Analytical conditions in all instruments were 15 kV accelerating voltage and a probe current of 12 nA; natural silicate and oxide minerals were used as standards. The data were reduced using ZAF (in JX8900 and JXA 8300) and phi-rho-z (in SX100) correction procedures. SiO_2, TiO_2, Al_2O_3, Cr_2O_3, FeO, MnO, MgO, CaO, Na_2O and K_2O were analysed for all samples. Representative mineral chemical data are given in Table 1 and a full dataset is provided in online Supplementary Table S1 (available at http://journals.cambridge.org/geo). Back-scattered images were taken (Fig. 2c) with a JEOL JX8900 electron probe micro-analyser at the Okayama University of Science with an accelerating voltage of 15 kv and a $2.387e^{-7}$ Å beam current.

3.b.1. *Chromite*

The chromites from the chromitite are weakly zoned. The Cr# (Cr/(Cr + Al)) varies over the range 0.59–0.69 and the Mg# ($Mg/(Mg + Fe^{2+})$) over 0.37–0.44, with little variation between cores and rims (Table 1).

3.b.2. *Mineral inclusions in chromite*

The chromite grains contain elongate orthopyroxene inclusions (Fig. 2c), which are slightly poor in SiO_2 (*c.* 53 wt %) and Al_2O_3 (*c.* 0.35 wt %) and weakly enriched in Cr_2O_3 (*c.* 1.37 wt. %) compared with the orthopyroxene in the matrix, which have SiO_2 (*c.* 57 wt %), Al_2O_3 (1.0–1.4 wt %) and Cr_2O_3 (0.05–0.15 wt %) (Fig. 2c, d).

3.b.3. *Silicate mineral chemistry*

In Ranomena chromitite the major intercumulus minerals are olivine and orthopyroxene. The olivine is highly magnesian forsterite with $F_{O92\text{-}93}$ (X_{Mg}= 0.92–0.93) and a low NiO content

https://doi.org/10.1017/S0016756816000972 Published online by Cambridge University Press

Table 1. Representative mineral chemistry of chromite, olivine and orthopyroxene from chromitites, Ranomena complex.

	Chromite core				
Analysis No.	160	169	224	245	384
SiO_2	0.10	0.00	0.00	0.00	0.01
TiO_2	0.34	0.27	0.58	0.55	0.59
Al_2O_3	17.05	16.26	16.17	15.12	15.25
Cr_2O_3	42.61	44.64	44.55	44.83	43.50
FeO	28.96	28.88	28.52	29.41	31.41
MnO	0.62	0.58	0.68	0.68	0.74
MgO	9.23	9.17	9.49	8.91	8.71
CaO	0.06	0.00	0.00	0.00	0.00
Na_2O	0.00	0.01	0.01	0.01	0.00
K_2O	0.05	0.00	0.05	0.01	0.02
NiO	0.06	0.21	0.07	0.12	0.11
Total	99.06	100.01	100.12	99.64	100.33
O			4		
Si	0.003	0.000	0.000	0.000	0.000
Ti	0.008	0.006	0.014	0.013	0.014
Al	0.650	0.618	0.612	0.580	0.582
Cr	1.089	1.138	1.132	1.154	1.113
Fe	0.783	0.779	0.766	0.801	0.850
Fe^{3+}	0.238	0.226	0.229	0.238	0.275
Fe^{2+}	0.569	0.576	0.560	0.587	0.605
Mn	0.017	0.016	0.018	0.019	0.020
Mg	0.445	0.441	0.455	0.432	0.420
Ca	0.002	0.000	0.000	0.000	0.000
Na	0.000	0.000	0.001	0.001	0.000
K	0.002	0.000	0.002	0.001	0.001
Ni	0.001	0.005	0.002	0.003	0.003
Total cation	3.001	3.005	3.002	3.003	3.003
Cr# (Cr/ Cr + Al)	0.626	0.648	0.649	0.665	0.657
Mg# (Mg/ Mg + Fe)	0.362	0.361	0.372	0.351	0.331
Al2O3 in melts	12.899	12.649	12.620	12.275	12.319
FeO/MgO in melts	1.790	1.783	1.710	1.826	1.899
	Orthopyroxene				
Analysis No.	334	326	319	344	325
SiO_2	57.27	56.99	56.90	56.76	57.49
TiO_2	0.09	0.07	0.08	0.04	0.07
Al_2O_3	1.13	1.05	1.20	1.37	1.02
Cr_2O_3	0.07	0.13	0.18	0.14	0.13
FeO	6.28	6.38	6.22	6.48	6.41
MnO	0.20	0.27	0.22	0.21	0.19
MgO	35.10	35.12	35.23	34.76	35.23
CaO	0.16	0.25	0.17	0.16	0.20
Na_2O	0.00	0.00	0.00	0.02	0.00
K_2O	0.00	0.01	0.04	0.00	0.02
NiO	0.04	0.03	0.01	0.00	0.02
Total	100.33	100.30	100.24	99.93	100.77
O			6		
Si	1.967	1.962	1.958	1.960	1.968
Ti	0.002	0.002	0.002	0.001	0.002
Al	0.046	0.043	0.049	0.056	0.041
Cr	0.002	0.004	0.005	0.004	0.003
Fe	0.180	0.184	0.179	0.187	0.184
Mn	0.006	0.008	0.006	0.006	0.006
Mg	1.797	1.802	1.807	1.789	1.797
Ca	0.006	0.009	0.006	0.006	0.007
Na	0.000	0.000	0.000	0.001	0.000
K	0.000	0.001	0.002	0.000	0.001
Ni	0.001	0.001	0.000	0.000	0.000
Total cation	4.007	4.014	4.014	4.010	4.009
Cr# (Cr/ Cr + Al)					
Mg# (Mg/ Mg + Fe)	0.909	0.908	0.910	0.905	0.907
Fs	0.091	0.092	0.090	0.094	0.092
En	0.906	0.903	0.907	0.902	0.904
Wo	0.003	0.005	0.003	0.003	0.004
	Olivine				
Analysis No.	375	355	356	357	358
SiO_2	40.65	41.05	41.32	41.01	40.76
TiO_2	0.00	0.01	0.01	0.00	0.01
Al_2O_3	0.02	0.00	0.03	0.00	0.00
Cr_2O_3	0.02	0.07	0.12	0.00	0.00
FeO	7.51	7.25	7.51	7.35	7.39
MnO	0.14	0.16	0.14	0.21	0.09

Table 1. Continued

	Olivine				
Analysis No.	375	355	356	357	358
MgO	50.81	51.95	51.42	51.41	51.17
CaO	0.01	0.00	0.00	0.00	0.00
Na_2O	0.00	0.01	0.00	0.00	0.01
K_2O	0.02	0.03	0.03	0.02	0.02
NiO	0.24	0.21	0.21	0.27	0.26
Total	99.43	100.73	100.78	100.28	99.71
O			4		
Si	0.993	0.989	0.995	0.993	0.992
Ti	0.000	0.000	0.000	0.000	0.000
Al	0.001	0.000	0.001	0.000	0.000
Cr	0.000	0.001	0.002	0.000	0.000
Fe	0.153	0.146	0.151	0.149	0.150
Mn	0.003	0.003	0.003	0.004	0.002
Mg	1.850	1.866	1.846	1.855	1.857
Ca	0.000	0.000	0.000	0.000	0.000
Na	0.000	0.001	0.000	0.000	0.001
K	0.001	0.001	0.001	0.001	0.001
Ni	0.004	0.004	0.004	0.005	0.005
Total cation	3.007	3.011	3.003	3.007	3.008
Mg# (Mg/ Mg + Fe)	0.923	0.927	0.924	0.926	0.925

(0.21–0.27 wt %). Orthopyroxene is highly magnesian enstatite that is depleted in iron (Mg# 0.90–0.91) and is slightly enriched in silica (52.00–57.80 wt %) (Table 1).

4. Discussion: petrogenesis and tectonic setting of the Ranomena complex

Many studies of ultramafic rocks have long established that chromite can be a useful petrogenetic and tectonic indicator (Irvine, 1967; Ahmed, Arai & Attia, 2001; Ahmed *et al.* 2005; Hellebrand *et al.* 2001, 2002). The composition of chromite depends strongly on its parental magma composition and its magma evolution (e.g. Irvine, 1965; Thayer, 1970; Roeder, 1994; Barnes & Roeder, 2001); the Cr# of chromite can therefore be used to calculate the degrees of partial melting experienced by ultramafic rocks (e.g. Dick & Bullen, 1984; Michael & Bonatti, 1985; Arai, 1994; Hellebrand *et al.* 2002). The Cr# of chromite increases with increasing degrees of melting, which reduces the Al contents of orthopyroxene and the host rock (Jaques & Green, 1980; Ohara & Ishi, 1998). Furthermore, the tectonic setting of a particular chromite can be evaluated by geochemical modelling of the liquidus chromite composition (e.g. Roeder & Reynolds, 1991). The application of chromite composition as a petrogenetic and geotectonic indicator therefore needs thorough petrographic and textural observations to recognize periods of magmatic and post-magmatic events experienced by the host rock (e.g. Rollinson, 1995; Suita & Streider, 1996).

4.a. Implications from chromite chemistry

The chromitite in the Ranomena complex has undergone greenschist to lower amphibolite facies metamorphism. A Cr/(Cr + Al) (Cr#) v.

https://doi.org/10.1017/S0016756816000972 Published online by Cambridge University Press

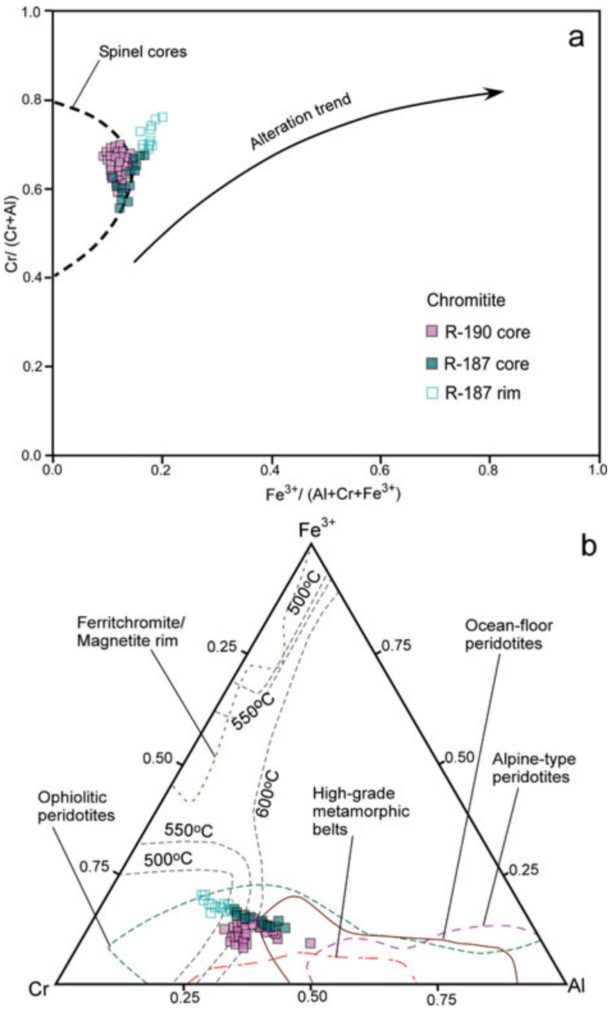

Figure 3. (Colour online) Mineral chemistry of chromite showing the effect of alteration. (a) $Cr/(Cr+Al)$ v. $Fe^{3+}/(Cr+Al+Fe^{3+})$ plot defining the alteration trend of the Ranomena chromites (modified after Ahmed *et al.* 2009). (b) The $Al–Cr–Fe^{3+}$ ternary diagram for chromite compositions from the Ranomena complex, which plot on the spinel stability boundary (Sack & Ghiorso, 1991), calculated for spinel in equilibrium with Fo_{90} olivine.

$Fe^{3+}/(Cr+Al+Fe^{3+})$ plot (Ahmed *et al.* 2009) (Fig. 3a) illustrates the alteration trend. All the chromite values from the Ranomena chromitite plot within the spinel core field (from Ahmed *et al.* 2009). The development of Fe^{3+}-enriched spinel is controlled by a decrease in size of the miscibility gap between a chromite core and a magnetite rim with increasing temperature (Barnes, 2000), where a complete solid solution between chromite and magnetite occurs at 600 °C. However, the compositions of the cores of chromite in the Ranomena chromitite plot outside the 600 °C field (the spinel stability field was calculated for equilibrium with Fo_{90} olivine) of Sack & Ghiorso (1991) (Fig. 3b). This indicates that the chromite cores were not affected by post-magmatic re-equilibration, and therefore preserve their primary compositions.

The alteration trend of the Ranomena chromites is shown in $Cr/(Cr+Al)$ v. $Fe^{3+}/(Cr+Al+Fe^{3+})$ space (Fig. 3a; Ahmed *et al.* 2009). On an $Al–Cr–Fe^{3+}$ ternary diagram (Fig. 3b; Jan & Windley, 1990; Barnes & Roeder, 2001) the rims of chromites plot in the Cr–Al field and the chromite cores in the ophiolite field. In a $Cr/(Cr+Al)$ v. $Mg/(Mg+Fe^{2+})$ diagram (Fig. 4a; after, Tamura & Arai, 2006; Oh *et al.* 2012) the chromites fall close to the peridotite field of a supra-subduction zone. On a TiO_2 v. Al_2O_3 diagram (Fig. 4b; Kamenetsky, Crawford & Meffre, 2001) the chromites plot in the arc field. The Al_2O_3 (wt %) v. Cr_2O_3 (wt %) relations of Franz & Wirth (2000) (Fig. 4c), which discriminate arc cumulate spinels from mantle arrays, suggest that the Ranomena chromite cores are arc cumulate spinels (Fig. 4c). In a Fe^{2+}/Fe^{3+} v. Al_2O_3 (wt %) plot (Fig. 4d) (after, Kamenetsky *et al.* 2001) the Ranomena chromites plot within the fields of supra-subduction zone peridotite and volcanic spinel. The low TiO_2 content also indicates that the ultramafic rocks formed in an arc-tectonic setting. In summary, the composition of chromite cores from the Ranomena chromitite indicates that they evolved in a supra-subduction zone arc setting (Fig. 4a–d) and the chromites have low NiO (*c.* 0.2 wt %), suggesting an ophiolitic origin (Fig. 5b).

4.b. Pressure–temperature estimations

Directly estimating the pressure and temperature of crystallization of mafic-ultramafic rocks is difficult, especially in metamorphosed rocks. We have therefore calculated empirically the *P–T* conditions of the Ranomena ultramafic rocks. Basu & McGregor (1975) proposed that the crystallization pressure of ultramafic rocks can be estimated using the relationship between Mg# and Cr# because there is a distinct variation of these parameters in chromite compositions between alkali-basalt and kimberlite xenoliths. Generally, chromite textures are related to their tectonic environments. The chromites from the Ranomena complex have a euhedral texture, which is a characteristic of spinels in xenoliths from kimberlite pipes. These euhedral spinels have higher $Cr/(Cr+Al)$ (0.62–0.68) and lower $Mg/(Mg+Fe^{2+})$ (0.40–0.44) ratios, which is a characteristic of euhedral spinels. The xenoliths from kimberlites have higher $Fe^{3+}/(Cr+Al+Fe^{3+})$ values than alkali olivine basalt xenoliths. The high $Cr/(Cr+Al+Fe^{3+})$ values also indicate that the spinels formed at a high pressure. The Ranomena chromites have $Cr/(Cr+Al+Fe^{3+})$ values ranging over 0.55–0.65, indicating a medium- to high-pressure origin. The chromites from the ultramafic rocks in this study plot very close to the kimberlite xenolith field in the Mg# v. Cr# diagram of Basu & McGregor (1975), suggesting a high-pressure (a minimum of 1.0 GPa) origin (Fig. 5a). The absence of plagioclase in the Ranomena ultramafic rocks suggests that the pressure conditions during crystallization were higher than those of the plagioclase peridotite field (e.g. Green & Ringwood, 1970; Schmidt & Poli, 1998). The estimated crystallization pressure at or over 1.0 GPa for the chromite corresponds to the melting

https://doi.org/10.1017/S0016756816000972 Published online by Cambridge University Press

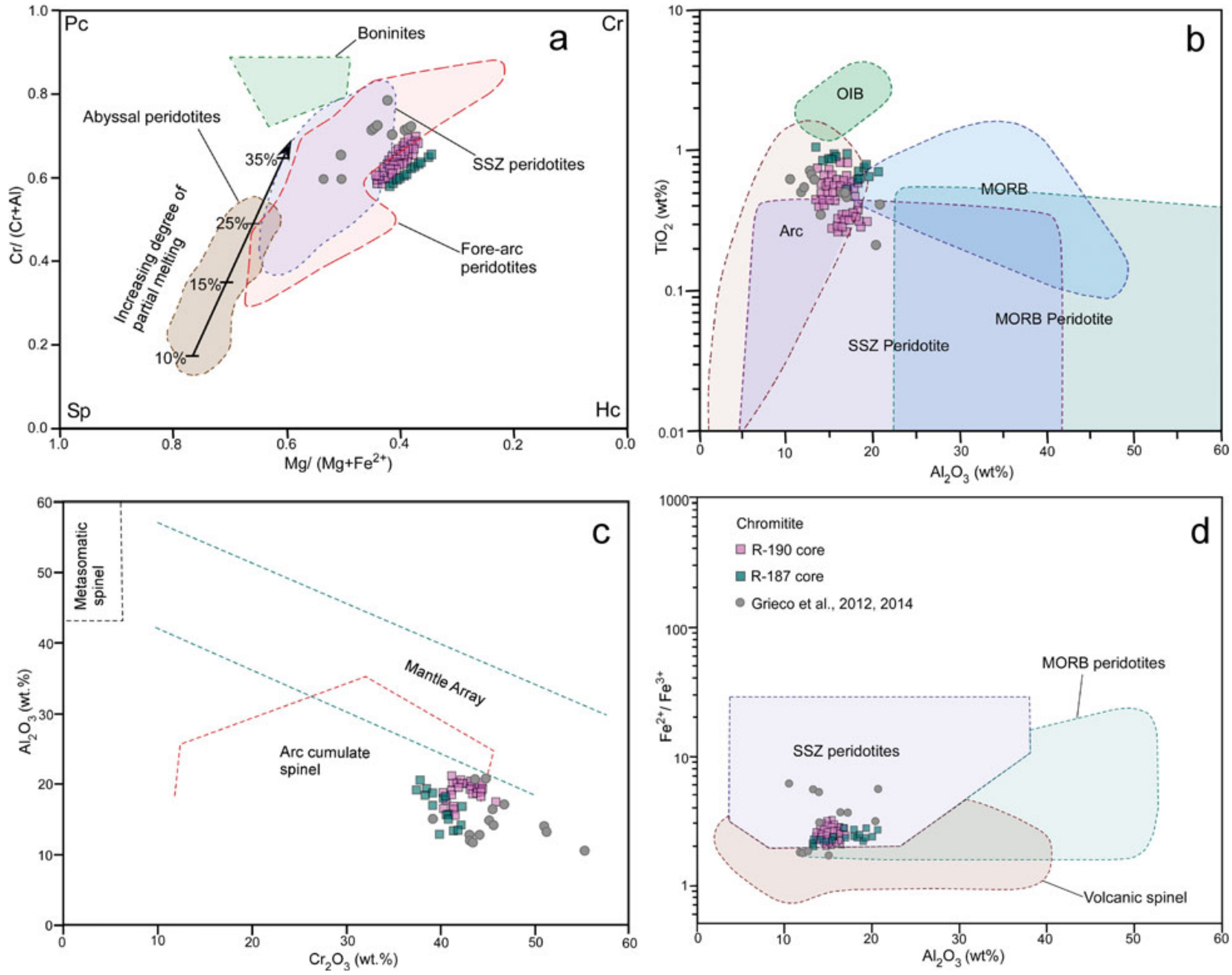

Figure 4. (Colour online) Tectonic discrimination diagrams for chromite. (a) Cr/(Cr + Al) v. Mg/(Mg + Fe^{2+}) (after Tamura & Arai, 2006; Oh *et al.* 2012). (b) TiO_2 (wt %) v. Al_2O_3 (after Kamenetsky *et al.* 2001). (c) Al_2O_3 (wt %) v. Cr_2O_3 (wt %) (after Franz & Wirth, 2000). (d) Fe^{2+}/ Fe^{3+} v. Al_2O_3 (wt %) (after Kamenetsky *et al.* 2001).

conditions in the spinel peridotite field (Dick & Bullen, 1984). To calculate the crystallization temperature, the Fe and Mg mole fractions of orthopyroxene were plotted in an experimentally contoured pyroxene quadrilateral (pyroxene-solvus thermometer of Lindsley, 1983) at 1.0 GPa. The orthopyroxenes from the Ranomena chromitite give a crystallization temperature of 1300-1250 °C (Lindsley, 1983) (Fig. 5c). This high value is interpreted as the igneous crystallization temperature of the residual mantle, and the lower temperature as a result of sub-solidus re-equilibration. The above results suggest that the Ranomena ultramafic rocks formed under upper mantle pressure and temperature conditions.

4.c. Parental magma composition

We used the mineral chemistry of the primary phases of chromite and clinopyroxene to determine the parental melt composition because the composition of chromite is strongly related to its parental melt composition, the degree of partial melting and its fractional crystallization (Irvine, 1977; Dick & Bullen, 1984; Barnes & Roeder, 2001). The Al_2O_3 content of chromite is commonly used to determine the nature of its parental melt and its ambient tectono-magmatic environment (e.g. Zhou *et al.* 1996; Kamenetsky *et al.* 2001; Rollinson, 2008; Zaccarini *et al.* 2011). The Al_2O_3 contents of melts in equilibrium with chromite (equilibrium at 1 bar) were calculated using the equation:

$$Al_2O_{3,\mathrm{spinel}} = 0.035 \times (Al_2O_{3,\mathrm{melt}})^{2.42}$$

as proposed by Maurel & Maurel (1982). The results indicate that the parental melts through which the Ranomena chromite crystallized had Al_2O_3 contents of 10.98–13.62 wt % (Table 1). Such high Al_2O_3 contents are representative of boninitic melts (Wilson, 1989) so the parental melts of the Ranomena chromitite had an arc parentage. The data indicate a high-Al nature of the parental magma and suggest that high-alumina basalt was the source magma. The parental melt data, along with the Al_2O_3 contents of chromite, plot very close to the evolutionary trend of an arc system in a diagram of Al_2O_3 in melt v. Al_2O_3 in spinel (Fig. 5d; Kamenetsky *et al.* 2001; Rollinson, 2008) and the trend extends towards a mid-ocean-ridge basalt (MORB) setting with increasing degrees of partial melting. The FeO/MgO

https://doi.org/10.1017/S0016756816000972 Published online by Cambridge University Press

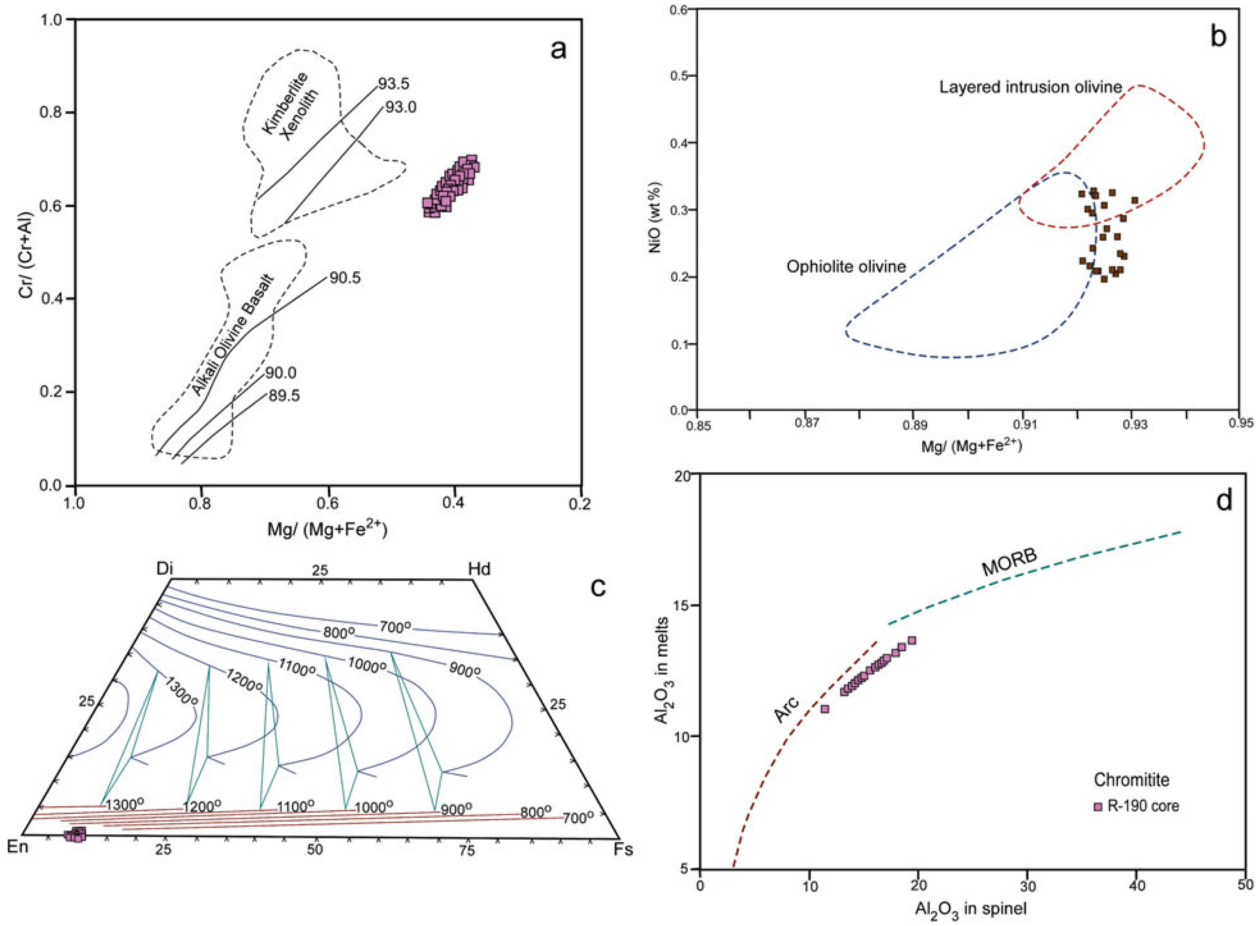

Figure 5. (Colour online) (a) Cr# v. Mg# diagram showing the discrimination between alkali-basalt and kimberlite xenoliths (after Basu & McGregor, 1975). The chromites from the Ranomena complex plot near the kimberlite xenolith field, suggesting a high-pressure origin. (b) Tectonic discrimination diagram based on the NiO v. $Mg/(Mg+Fe^{2+})$ of chromites from Ranomena chromitites (Fields are after, Rehfeldt *et al.* 2007). (c) Orthopyroxene composition from the Ranomena complex in an experimentally contoured Ca–Mg–Fe phase-relation diagram at 1.0 GPa (after Lindsley, 1983). (d) Al_2O_3 in melts v. Al_2O_3 in spinel (after, Rollinson, 2008), based on melt calculations of Maurel & Maurel (1982).

ratio of a parental melt in equilibrium with chromite at 1 kbar can also be estimated from a chromite composition using the equation:

$$\ln\left(\frac{FeO}{MgO}\right)_{\text{spinel}} = 0.47 - 1.07Y_{\text{spinel, Al}} + 0.64Y_{\text{spinel, Fe}^{3+}} + \ln\left(\frac{FeO}{MgO}\right)_{\text{liquid}}$$

where FeO and MgO are in wt % and

$$Y_{\text{spinel, Al}} = \frac{Al}{Al + Cr + Fe^{3+}} \quad \text{and}$$

$$Y_{\text{spinel, Fe}^{3+}} = \frac{Fe^{3+}}{Al + Cr + Fe^{3+}}$$

as proposed by Maurel & Maurel (1982). The results show that the parental magma from which the chromite crystallized had a FeO/MgO ratio of 0.9–1.8. Boninites have a FeO/MgO ratio over the range 0.7–1.4, whereas the same ratio in MOR basalts varies over 1.2–1.6, suggesting the Ranomena chromite had an arc derivation. The parental magma was therefore Al- and Fe-rich and is comparable to the chemical characteristics of a tholeiitic basalt magma. Based on all the above lines of evidence, we suggest that the composition of the parental magma of the Ranomena ultramafic rocks was similar to that of a primitive tholeiitic basalt formed by a high degree of partial melting of a mantle peridotite. These results indicate that the parental melt had a composition equivalent to that of an island-arc tholeiite (IAT).

Regarding the origin of chromitite, Irvine (1977) suggested that the mixing of a chemically primitive mafic melt with a more evolved mafic melt could produce a hybrid magma from which chromitite layers could crystallize. The Ranomena chromitite is characterized by a massive texture. González-Jiménez *et al.* (2014*a*) proposed that disseminated chromitite can form with a low melt/rock ratio and massive chromitite with a high melt/rock ratio. A high abundance of olivine facilitates movement of melt along grain boundaries and enhances the formation of three-dimensional networks of olivine to form disseminated chromitite, whereas melts from different provenances with different physico-chemical properties such as SiO_2 content,

https://doi.org/10.1017/S0016756816000972 Published online by Cambridge University Press

viscosity, density and temperature inter-mix and give rise to nodular and orbicular chromitite, which continues to grow forming massive chromitite González-Jiménez *et al.* (2014*a*).

5. Conclusions

The main conclusions of this study are as follows.

1. The composition of orthopyroxene from the Ranomena chromitite indicates a crystallization temperature range of 1250–1300 °C at 1.0 GPa.
2. Melt calculations using chromite cores show that the composition of the parental magma of the Ranomena complex was similar to that of a primitive tholeiitic basalt formed by a high degree of mantle melting.
3. The chemistry of chromite in chromitite from the Ranomena complex indicates that it formed in a supra-subduction zone arc tectonic setting.

Acknowledgements. This study is a contribution to ISRO-IISc Space Technology Cell projects ISTC/MES/SK/232 and ISTC/CEAS/SJK/291. We are grateful to the Ministry of Earth Sciences, Government of India (project MoES/ATMOS/PP-IX/09) for laboratory facilities. We utilized the Electron Micro-Probe facility at the Advanced Facility for Microscopy and Micro-analysis, IISc, Bangalore, Electron Probe Micro Analysis Laboratory, CSIR-NGRI, Hyderabad and thank Mr Anil Kaushik for his support. EVSSKB thanks the Director, CSIR-NGRI for permission to work with this project supported by MLP-6513-28-EVB and INDEX-WP-2.1.

Supplementary material

To view supplementary material for this article, please visit https://doi.org/10.1017/S0016756816000972.

References

Ahmed, A. H., Arai, S. & Attia, A. K. 2001. Petrological characteristics of podiform chromitites and associated peridotites of the Pan-African ophiolite complexes of Egypt. *Mineralium Deposita* **36**, 72–84.

Ahmed, A. H., Arai, S., Yaser, M. A., Ikenne, M. & Rahimi, A. 2009. Platinum-group elements distribution and spinel composition in podiform chromitites and associated rocks from the upper mantle section of the Neoproterozoic Bou Azzer ophiolite, Anti-Atlas, Morocco. *Journal of African Earth Sciences* **55**, 92–104.

Ahmed, A. H., Arai, S., Yaser, M. A. & Rahimi, A. 2005. Spinel composition as a petrogenetic indicator of the mantle section in the Neoproterozoic Bou Azzer ophiolite, Anti-Atlas, Morocco. *Precambrian Research* **138**, 225–34.

Arai, S. 1980. Dunite-harzburgite-chromitite complexes as refractory residue in the Sangun-Yamaguchi zone, western Japan. *Journal of Petrology* **21**, 141–65.

Arai, S. 1992. Chemistry of Cr-spinel in volcanic rocks a potential guide to magma chemistry. *Mineralogical Magazine* **56**, 173–84.

Arai, S. 1994. Characterization of spinel peridotites by olivine-spinel compositional relationships: review and interpretation. *Chemical Geology* **113**, 191–204.

Arai, S., Okamura, H., Kadoshima, K., Tanaka, C., Suzuki, S. & Ishimaru, S. 2011. Chemical characteristics of Cr-spinel in plutonic rocks: implications for deep magma processes and discrimination of tectonic setting. *Island Arc* **20**, 125–37.

Aswad, K. J. A., Aziz, N. R. H. & Koyi, H. A. 2011. Cr-spinel compositions in serpentinites and their implications for the petrotectonic history of the Zagros Suture Zone, Kurdistan Region, Iraq. *Geological Magazine* **148**, 802–18.

Barnes, S. J. 2000. Cr-spinel in komatiites, II. Modification during greenschist to mid-amphibolite facies metamorphism. *Journal of Petrology* **41**, 387–409.

Barnes, S. J. & Hill, R. E. T. 1995. Poikilitic Cr-spinel in komatiitic cumulates. *Geochimica Cosmochimica Acta* **39**, 937–45.

Barnes, S. J. & Roeder, P. L. 2001. The range of spinel compositions in terrestrial mafic and ultramafic rocks. *Journal of Petrology* **42**, 2279–302.

Basu, A. R. & McGregor, I. O. 1975. Chromite spinels from ultramafic xenoliths. *Geochimica Cosmochimica Acta* **39**, 937–45.

Bauer, W. & Key, R. 2005. Carte Géologique Préliminaire de Madagascar. 1:500000. Toamasina No 6. British Geological Survey, Keyworth, UK.

Besairie, H. 1967. The precambrian of madagascar. In *The Precambrian*, volume 3 (ed K. Rankama), pp. 133–42. Wiley, Chichester.

Besairie, H. 1970. *Descriptions Géologiques du Massif Ancien de Madagascar. Déuxieme Volume: La Région Côtière Orientale entre le Mangoro et Vangaindrano*. Tananarive: Documentation du Bureau Géologique de Madagascar, 67 pp.

Burkhard, D. J. M. 1993. Accessory Cr-spinels: their coexistence and alteration in serpentinites. *Geochimica Cosmochimica Acta* **55**, 1297–306.

Cameron, E. N. 1975. Post-cumulus and subsolidus equilibration of Cr-spinel and coexisting silicates in the Eastern Bushveld Complex. *Geochimica Cosmochimica Acta* **39**, 1021–33.

Collins, A. S., Fitzsimons, I. C. W., Hulscher, B. & Razakamanana, T. 2003. Structure of the eastern margin of the East African Orogen in central Madagascar. *Precambrian Research* **123**, 111–33.

Collins, A. S. & Windley, B. F. 2002. The tectonic evolution of central and northern Madagascar and its place in the final assembly of Gondwana. *Journal of Geology* **110**, 325–40.

Dharma Rao, C. V., Santosh, M., Sajeev, K. & Windley, B. F. 2013. Cr-spinel-silicate chemistry of the Neoarchean Sittampundi Complex, southern India: implications for subduction-related arc magmatism. *Precambrian Research* **227**, 259–75.

Dick, H. J. B. & Bullen, T. 1984. Cr-spinel as a petrogenetic indicator in abyssal and alpine-type peridotites and spatially associated lavas. *Contributions to Mineralogy and Petrology* **86**, 54–76.

Eales, H. V., Wilson, A. H. & Reynolds, I. M. 1988. Complex unmixed spinels in layered intrusions within an obducted ophiolite in the Natal-Namaqua mobile belt. *Mineralium Deposita* **23**, 150–7.

Evans, B. W. & Frost, B. R. 1975. Chrome-spinel in progressive metamorphism: a preliminary analysis. *Geochimica Cosmochimica Acta* **39**, 959–72.

Franz, L. & Wirth, R. 2000. Spinel inclusions in olivine of peridotite xenoliths from TUBAF seamount (Bismarck Archipelago/Papua New Guinea): evidence for the thermal and tectonic evolution of oceanic lithosphere. *Contributions to Mineralogy and Petrology* **140**, 283–95.

González-Jiménez, J. M., Griffin, W. L., Gervilla, F., Proenza, J. A., O'Reilly, S. Y., Akbulut, M., Pearson, N. J. & Arai, S. 2014a. Chromitites in ophiolites: How, where, when, why? Part II. The crystallization of chromitites. *Lithos* **189**, 140–58.

González-Jiménez, J. M., Griffin, W. L., Gervilla, F., Proenza, J. A., O'Reilly, S. Y. & Pearson, N. J. 2014b. Chromitites in ophiolites: How, where, when, why? Part I. A review and new ideas on the origin and significance of platinum-group minerals. *Lithos* **189**, 127–39.

González-Jiménez, J. M., Locmelis, M., Belousova, E., Griffin, W. L., Gervilla, F., Kerestedjian, T. N., O'Reilly, S. Y., Pearson, N. J. & Sergeeva, I. 2015. Genesis and Tectonic implications of podiform chromitites in the metamorphic ultramafic massif of Dobromirsti (Bulgaria). *Gondwana Research* **27**, 555–74.

Green, D. H. & Ringwood, A. E. 1970. Mineralogy of peridotite compositions under mantle conditions. *Physics of Earth and Planetary Interiors* **8**, 359–71.

Grieco, G., Merlini, A. & Cazzaniga, A. 2012. The tectonic significance of PGM-bearing chromitites at the Ranomena mine, Toamasina Cr-spinel district, Madagascar. *Ore Geology Reviews* **44**, 70–81.

Grieco, G., Merlini, A., Pedrottia, M., Moronia, M. & Randrianja, R. 2014. The origin of Madagascar chromitites. *Ore Geology Reviews* **58**, 55–67.

Hamlyn, P. R. & Keays, R. R. 1979. Origin of Cr-spinel compositional variation in the Panton Sill, Western Australia. *Contributions to Mineralogy and Petrology* **69**, 75–82.

Hellebrand, E., Snow, J. E., Dick, H. J. B. & Hoffmann, A. W. 2001. Coupled major and trace elements as indicators of the extent of melting in mid-ocean-ridge peridotites. *Nature* **410**, 677–81.

Hellebrand, E., Snow, J. E., Hoppe, P. & Hofmann, A. W. 2002. Garnet-field melting and late-stage refertilization in 'Residual' abyssal peridotites from the Central Indian Ridge. *Journal of Petrology* **43**, 2305–38.

Hottin, G. 1969. Les terrains cristallins du centre-nord et du nord-est de Madagascar. *Document du Bureau Géologique de Madagascar* **178** (2 volumes), 1–192; 193–381.

Irvine, T. N. 1965. Cr-spinel as a petrogenetic indicator: Part 1. Theory. *Canadian Journal of Earth Sciences* **2**, 648–72.

Irvine, T. N. 1967. Cr-spinel as a petrogenetic indicator, Part II. Petrological applications. *Canadian Journal of Earth Sciences* **4**, 71–103.

Irvine, T. N. 1977. Origin of Cr-spinel layers in the Muskoka intrusion and other intrusions: a new interpretation. *Geology* **5**, 273–7.

Ishwar-Kumar, C., Rajesh, V. J., Windley, B. F., Razakamanana, T., Itaya, T., Babu, E. V. S. S. K., Sajeev, K. 2016a. Petrogenesis and tectonic setting of the Bondla mafic-ultramafic complex, western India: Inferences from chromian spinel chemistry. *Journal of Asian Earth Sciences*, published online 5 July 2016, doi: 10.1016/j.jseaes.2016.07.004.

Ishwar-Kumar, C., Sajeev, K., Windley, B. F., Kusky, T. M., Feng, P., Ratheesh-Kumar, R. T., Huang, Y., Zhang, Y., Jiang, X., Razakamanana, T., Yagi, K. & Itaya, T. 2015. Evolution of high-pressure mafic granulites and pelitic gneisses from NE Madagascar: Tectonic implications. *Tectonophysics* **662**, 219–42.

Ishwar-Kumar, C., Santosh, M., Wilde, S. A., Tsunogae, T., Itaya, T., Windley, B. F. & Sajeev, K. 2016b. Mesoproterozoic suturing of Archean crustal blocks in western peninsular India: Implications for India-Madagascar correlations. *Lithos* **263**, 143–60, doi: 10.1016/j.lithos.2016.01.016.

Ishwar-Kumar, C., Windley, B. F., Horie, K., Kato, T., Hokada, T., Itaya, T., Yagi, K., Gouzu, C. & Sajeev, K. 2013. A Rodinian suture in western India: New insights on India-Madagascar correlations. *Precambrian Research* **236**, 227–51.

Jan, M. Q. & Windley, B. F. 1990. Cr-spinel-silicate chemistry in ultramafic rocks of the Jijal Complex, northwest Pakistan. *Journal of Petrology* **31**, 67–71.

Jaques, A. L. & Green, D. H. 1980. Anhydrous melting of peridotite at 0–15 kb pressure and the genesis of tholeiitic basalts. *Contributions to Mineralogy and Petrology* **73**, 287–310.

Kamenetsky, V., Crawford, A. J. & Meffre, S. 2001. Factors controlling chemistry of magmatic spinel: an empirical study of associated olivine, Cr-spinel and melt inclusions from primitive rocks. *Journal of Petrology* **42**, 655–71.

Karipi, S., Tsikouras, B., Hatzipanagiotou, K. & Grammatikopoulos, T. A. 2007. Petrogenetic significance of spinel-group minerals from the ultramafic rocks of the Iti and Kallidromon ophiolites (Central Greece). *Lithos* **99**, 136–49.

Key, R. M., Pitfield, P. E. J., *et al.* 2011. Polyphase Neoproterozoic orogenesis within the East Africa-Antarctica orogenic belt in central and northern Madagascar. In *The Formation and Evolution of Africa: A Synopsis of 3.8 Ga of Earth History* (eds D. J. J. van Hinsbergen, S. J. H. Buiter, T. H. Torsvik, C. Gaina & S. J. Webb), pp. 49–68. Geological Society of London, Special Publication no. 357.

Kröner, A., Hegner, E., Collins, A. S., Windley, B. F., Brewer, T. S., Razakamanana, T. & Pidgeon, R. T. 2000. Age and magmatic history of the Antananarivo block, Central Madagascar, as derived from zircon geochronology and Nd isotopic systematics. *American Journal of Science* **300**, 251–88.

Kröner, A., Windley, B. F., Jaeckel, P., Brewer, T. S. & Razakamanana, T. 1999. New zircon ages and regional significance for the evolution of the Pan-African orogen in Madagascar. *Journal of the Geological Society of London* **156**, 1125–35.

Lindsley, D. H. 1983. Pyroxene thermometry. *American Mineralogist* **68**, 477–93.

Maurel, C. & Maurel, P. 1982. Étude experimental de la distribution de l'aluminium entre bain silicate basique et spinel chromifère. Implications pétrogenetiques: tenore en chrome des spinelles. *Bulletin de Minéralogie* **105**, 197–202.

Michael, P. J. & Bonatti, E. 1985. Petrology of ultramafic rocks from Sites 556, 558, and 560 in the North Atlantic. In *Initial Reports Deep Sea Drilling Project*, volume 82 (eds H. Bougault, S. C. Cand et al.), pp. 523–8. Washington.

Mukherjee, R., Mondal, S. K., Rosing, M. T. & Frei, R. 2010. Compositional variations in the Mesoarchean Cr-spinels of the Nuggihalli schist belt, Western Dharwar Craton (India): potential parental melts and implications for tectonic setting. *Contributions to Mineralogy and Petrology* **160**, 865–85.

Oh, C. W., Seo, J., Choi, S. G., Rajesh, V. J. & Lee, J. H. 2012. U-Pb SHRIMP zircon geochronology, petrogenesis, and tectonic setting of the Neoproterozoic Baekdong ultramafic rocks in the Hongseong Collision belt, South Korea. *Lithos* **128–131**, 100–12.

Ohara, Y. & Ishi, T. 1998. Peridotites from the southern Mariana fore-arc: heterogeneous fluid supply in mantle wedge. *Island Arc* **7**, 541–58.

Raharimahefa, T. & Kusky, T. M. 2009. Structural and remote sensing analysis of the Betsimisaraka Suture in northeastern Madagascar. *Gondwana Research* **15**, 14–27.

Ratheesh-Kumar, R. T., Ishwar-Kumar, C., Windley, B. F., Razakamanana, T., Nair, R. R. & Sajeev, K. 2015. India-Madagascar paleo-fit based on flextural isostasy of their rifted margins. *Gondwana Research* **27**, 581–600.

Rehfeldt, T., Dorrit, E. J., Carlson, R. W. & Foley, S. F. 2007. Fe-rich dunite xenoliths from South African kimberlites: cumulates from Karoo flood basalts. *Journal of Petrology* **48**, 1387–409.

Rekha, S., Bhattacharya, A. & Prabhakar, N. 2014. Tectonic restoration of the Precambrian crystalline rocks along the west coast of India: correlation with eastern Madagascar in East Gondwana. *Precambrian Research* **252**, 191–208.

Rekha, S., Viswanath, T. A., Bhattacharya, A. & Prabhakar, N. 2013. Meso/Neoarchean crustal domains along the north Konkan coast, western India: The Western Dharwar Craton and the Antongil-Masora Block (NE Madagascar) connection. *Precambrian Research* **233**, 316–36.

Roeder, P. L. 1994. Chromite: from the fiery rain of chondrules to the Kilauea Iki lava lake. *Canadian Mineralogist* **32**, 729–46.

Roeder, P. L., Campbell, I. H. & Jamieson, H. E. 1979. A re-evaluation of the olivine-spinel geothermometer. *Contributions to Mineralogy and Petrology* **68**, 325–34.

Roeder, P. L. & Reynolds, I. 1991. Crystallization of Cr-spinel and chromium stability in basaltic melts. *Journal of Petrology* **32**, 909–34.

Rollinson, H. 1995. The relationship between Cr-spinel chemistry and the tectonic setting of Archaean ultramafic rocks. In *Sub-Saharan Economic Geology* (eds T. G. Blenkinshop & P. Tromps), pp. 7–23. Amsterdam: Balkema.

Rollinson, H. 2008. The geochemistry of mantle chromitite from the northern part of the Oman ophiolite: inferred parental melt compositions. *Contributions to Mineralogy and Petrology* **156**, 273–88.

Rollinson, H., Appel, P. W. U. & Frie, R. 2002. A metamorphosed, early Archaean chromitite from West Greenland: implications for the genesis of Archaean anorthositic chromitites. *Journal of Petrology* **43**, 2143–70.

Sack, R. O. & Ghiorso, M. S. 1991. Cr-spinels as petrogenetic indicators: thermodynamic and petrological applications. *American Mineralogist* **76**, 827–47.

Schmidt, M. W. & Poli, S. 1998. Experimentally based water budget for dehydrating slabs and consequences for arc magma generation. *Earth and Planetary Science Letters* **163**, 361–79.

Schofield, D. I., Thomas, R. J. *et al*. 2010. Geological evolution of the Antongil craton, NE Madagascar. *Precambrian Research* **182**, 187–203.

Scowen, P. A. H., Roeder, P. L. & Heltz, R. T. 1991. Reequilibration of Cr-spinel within Kilauea Iki lava lake, Hawaii. *Contributions to Mineralogy and Petrology* **107**, 8–20.

Suita, M. T. & Streider, A. J. 1996. Cr-spinels from Brazilian mafic-ultramafic complexes: metamorphic modifications. *International Geology Review* **38**, 245–67.

Tamura, A. & Arai, S. 2006. Harzburgite-dunite-orthopyroxenite suite as a record of supra-subduction zone setting for the Oman ophiolite mantle. *Lithos* **90**, 43–56.

Thayer, T. P. 1970. Cr-spinel segregations as petrogenetic indicators. *Geological Society of Africa Special Publications* **1**, 381–90.

Tsujimori, T., Esaka, N., Abimbola, A. F., Nishido, H., Ninagawa, K. & Itaya, T. 1998. Quantitative analysis of common rock-forming minerals by a modern wavelength-dispersive type EPMA: a preliminary report. *Bulletin of the Research Institute of Natural Sciences, Okayama University of Science* **23**, 51–60.

Tucker, R. D., Ashwal, L. D., Handke, M. J., Hamilton, M. A., Legrange, M. & Rambeloson, R. A. 1999. U-Pb geochronology and isotope geochemistry of the Archean and Proterozoic rocks of north-central Madagascar. *Journal of Geology* **107**, 135–53.

Tucker, R. D., Roig, J. Y., Delor, C., Amerlin, Y., Goncalves, P., Rabarimanana, M. H., Ralison, A. V. & Belcvher, R. W. 2011. Neoproterozoic extension in the Greater Dharwar Craton: a reevaluation of the 'Betsimisaraka suture' in Madagascar. *Canadian Journal of Earth Sciences* **48**, 389–417.

Tucker, R. D., Roig, J. Y., Moine, B., Delor, C. & Peters, S. G. 2014. A geological synthesis of the Precambrian shield in Madagascar. *Journal of African Earth Sciences* **94**, 9–30.

Wilson, M. 1989. *Igneous Petrogenesis*. London: Unwin Hyman, 446 pp.

Windley, B. F., Razafiniparany, A., Razakamanana, T. & Ackermand, D. 1994. Tectonic framework of the Precambrian of Madagascar and its Gondwana connections: a review and reappraisal. *Geologisch Rundschau* **83**, 642–59.

Zaccarini, F., Garuti, G., Proenza, J. A., Campos, L., Thalhammer, O. A. R., Aiglsperger, T. & Lewis, J. F. 2011. Cr-spinel and platinum group elements mineralization in the Santa Elena ultramafic nappe (Costa Rica): geodynamic implications. *Geologica Acta* **9**, 1–17.

Zhou, M., Robinson, P. T., Malpas, J. & Li, Z. 1996. Podiform chromitites in the Luobusa ophiolite (southern Tibet): implications for melt/rock interaction and Cr-spinel segregation in the upper mantle. *Journal of Petrology* **37**, 3–21.

Zhou, M., Robinson, P. T., Su, B., Gao, J., Li, J., Yang, J. & Malpas, J. 2014. Compositions of Cr-spinel, associated minerals, and parental magmas of podiform Cr-spinel deposits: The role of slab contamination of asthenospheric melts in suprasubduction zone environments. *Gondwana Research* **26**, 262–83.